Article

MnB$_6^-$: An Open-Shell Metallaboron Analog of 3d Metallabenzenes

Published as part of The Journal of Physical Chemistry virtual special issue "International Symposium on Molecular Spectroscopy".

Ling Fung Cheung, G. Stephen Kocheril, Joseph Czekner, and Lai-Sheng Wang*

Read Online

ACCESS | Metrics & More | Article Recommendations | SI Supporting Information

ABSTRACT: We report a study of the structure and bonding of a transition-metal-doped boron cluster, MnB$_6^-$, using high-resolution photoelectron imaging and quantum chemical calculations. Vibrationally resolved photoelectron spectra indicate a significant geometry change between the anionic and neutral ground states of MnB$_6$. The electron affinity of MnB$_6$ is measured to be 2.4591(5) eV, and vibrational frequencies for five of its vibrational modes were determined. The experimental data are combined with theoretical calculations to determine the structure and bonding of MnB$_6^-$, which is found to be planar with a B-centered hexagonal structure (C_{2v} symmetry) and a quintet spin state ($^5A_2$). Nuclear-independent chemical shift calculations indicate that MnB$_6^-$ is aromatic. Molecular orbital analyses reveal that MnB$_6^-$ contains three π orbitals, one of which is singly occupied. Hence, MnB$_6^-$ can be considered as an open-shell metallaboron analog of 3d metallabenzenes.
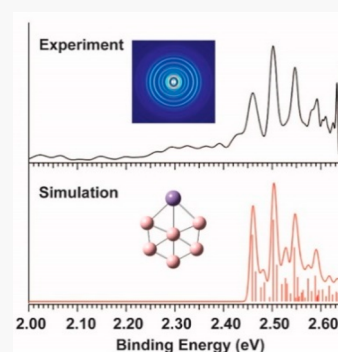
INTRODUCTION

Boron is known to form three-dimensional (3D) polyhedral structures with delocalized bonds in many borane compounds because of its electron deficiency.[1] The structures and bonding of bare boron clusters have been extensively investigated by joint experimental and computational studies in recent years.[2−8] The structures of small boron clusters have been found to be predominantly planar with delocalized bonding, giving rise to both σ and π aromaticity.[9−15] It was further found that the planarity and aromaticity of small boron clusters obey the Hückel rule. Transition-metal-doped boron clusters have also been studied by joint photoelectron spectroscopy (PES) and computational chemistry.[16−26] In addition, there has been a variety of computational studies on transition-metal-doped boron clusters.[27−35] Notably, a class of aromatic borometallic molecular wheels (M©B$_n^-$) ($n = 8−10$) have been experimentally discovered.[16,17] While Re©B$_8^-$ and Re©B$_9^-$ have been found to belong to the class of borometallic molecular wheels,[36] a recent study showed that ReB$_6^-$ is planar with the Re atom being on the periphery of the cluster.[37] Chemical bonding analyses revealed that ReB$_6^-$ is aromatic with six π electrons, whereas AlB$_6^-$ with four π electrons is antiaromatic with an out-of-plane distortion. The bonding in ReB$_6^-$ was further shown to be similar to that in rhenabenzene. Thus, ReB$_6^-$ is the first aromatic metallaboron analog of metallabenzenes.[37]

Metallabenzenes are a class of organometallic compounds in which one CH group in benzene is substituted by a metal atom.[38−41] There have been increasing studies on metallabenzenes due to their interesting chemical and structural properties. While there have been numerous reports on the syntheses of metallabenzenes with various 5d transition metals,[39−47] as well as the 4d ruthenium,[48,49] it has been challenging to synthesize metallabenzenes with the first-row and other second-row transition metals.[40,50] Very recently, a tetralithio metalla-aromatic compound has been synthesized with two five-membered manganacycles spiro-fused by a high-spin Mn atom.[51] However, the synthesis of monocyclic metallabenzenes with any 3d transition metals has remained elusive, although there has been a previous theoretical study.[52]

In this article, we address the possibility of producing a 3d metallaboron analog of metallabenzenes. We report an investigation of a 3d transition-metal metallaboron cluster, MnB$_6^-$, produced by laser vaporization of a mixed Mn/B target. The selection of Mn was inspired by the recent synthesis of manganacycles[51] and the ReB$_6^-$ metallaboron analog of 5d metallabenezenes.[37] High-resolution photoelectron imaging (PEI) in conjunction with computational chemistry has shown that MnB$_6^-$ has a planar structure with the Mn atom on the periphery of the cluster, similar to that of ReB$_6^-$. However, the MnB$_6^-$ cluster has a high spin ground state ($^5A_2$) and displays relatively weak Mn−B interactions. Nuclear shielding calculations using the nuclear-independent
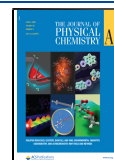
chemical shift (NICS) reveal aromatic characters in MnB_6^-, which can be considered as a metallaboron analog of metallabenzenes with a 3d transition metal atom.

■ EXPERIMENTAL AND THEORETICAL METHODS

High-Resolution Photoelectron Imaging. The experiment was carried out using a high-resolution PEI apparatus with a laser vaporization cluster source, which has been described in detail previously.[53] Briefly, we produced MnB_6^- by focusing the second harmonic of a Nd:YAG laser onto a disk target, which was made of a mixture of isotopically enriched ^{10}B, Mn, and Ag powders (Ag served as a binder). The laser-induced plasma was quenched by a helium carrier gas seeded with 10% argon, initiating nucleation. The nascent clusters were entrained in the carrier gas and underwent a supersonic expansion, producing a cold cluster beam. Anionic clusters were extracted perpendicularly into a time-of-flight mass spectrometer. The MnB_6^- cluster of current interest was mass-selected into the interaction zone of the velocity-map imaging (VMI) system.

A second Nd:YAG laser or a Deyang Tech dye laser pumped by a Nd:YAG laser was used to photodetach the size-selected MnB_6^- clusters. The photoelectrons were extracted from the interaction zone and focused onto a set of microchannel plates coupled with a phosphor screen and a charge-coupled device camera. Each experiment at a given photon energy required about 100 000 to 200 000 laser shots to achieve reasonable signal-to-noise ratios. The VMI lens was calibrated using the photoelectron images of Au^- and Bi^- at various photon energies. The photoelectron images were analyzed using the maximum entropy method (MEVIR and MEVELER).[54] The typical energy resolution of the VMI system was ∼0.6% for high kinetic energy electrons and could be as good as 1.2 cm^{-1} for low kinetic energy electrons.[53]

Theoretical Methods. Structural searches for MnB_6^- were performed by direct Monte Carlo sampling with local optimization. Around 2000 different structures with various spin multiplicities (singlet, triplet, quintet, and septet) were randomly generated and optimized at the PBE/6-31G* level of theory.[55−57] Low-lying isomers within 1 eV of the global minima were further optimized at the B3LYP/6-311+G* level of theory.[58] The adiabatic detachment energy (ADE) for the ground state transition was calculated as the energy difference between the optimized anion and its corresponding neutral. Franck−Condon simulation was performed using ezSpectrum.[59] NICS calculations were carried out at the B3LYP/6-311+G* level of theory.[60] All calculations were done using Gaussian 09.[61]

■ RESULTS

Experimental Results. Figure 1 shows the PE images and spectra of MnB_6^- at five different photon energies. The first sharp peak labeled as X denotes the 0−0 transition, corresponding to the transition from the anion ground state to that of the neutral. Peak X defines the electron affinity (EA) of MnB_6^- to be 2.4591 ± 0.0005 eV. Extensive vibrational structures were resolved, indicating a significant geometry change between the ground states of the anion and the neutral system. The resolved vibrational peaks are labeled as a−j. The binding energies of the observed peaks and their assignments are summarized in Table 1. The weak signals on the lower binding energy side of peak X were likely due to vibrational hot
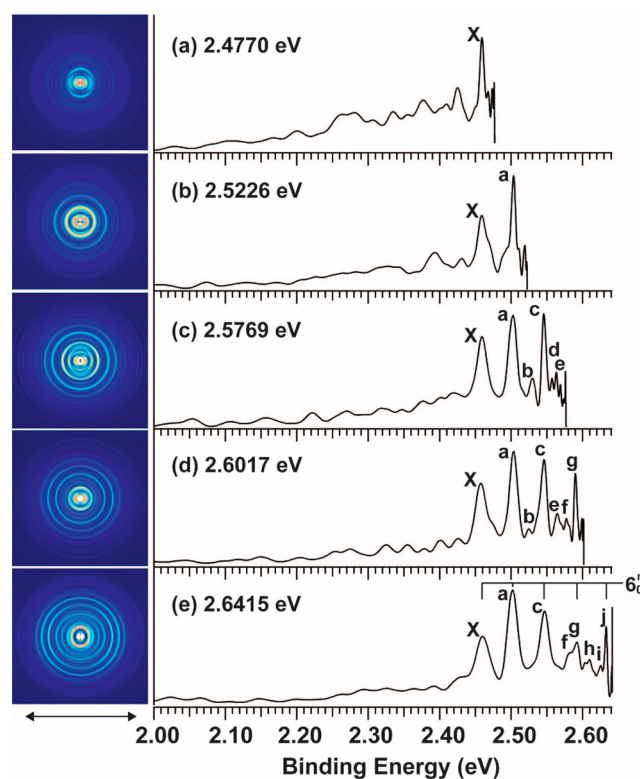

Figure 1. Photoelectron images and spectra of MnB_6^- at five different photon energies. The double arrows below the images denote the laser polarization.

Table 1. Measured Binding Energies (BE), Energy Shifts Relative to the 0-0 Transition, and Assignments of the Observed Vibrational Peaks in the PE Spectra of MnB_6^- and Comparison with the Theoretical Frequencies Computed at the B3LYP/6-311+G* Level of Theory

	experimental			theoretical[a]
peak	BE (eV)	assignment	energy shift (cm^{-1})	frequency (cm^{-1})
X	2.4591(5)	0_0^0		
a	2.5035(9)	6_0^1	358(9)	348
b	2.5292(23)	5_0^1	565(19)	578
c	2.5461(10)	6_0^2	702(9)	
d	2.5569(16)	4_0^1	789(14)	733
e	2.5633(13)	3_0^1	840(11)	818
f	2.5777(18)	$5_0^1 6_0^1$	957(15)	
g	2.5901(13)	6_0^3	1057(11)	
h	2.6099(18)	1_0^1	1216(15)	1225
i	2.6259(35)	$4_0^1 5_0^1$	1345(29)	
j	2.6330(12)	6_0^4	1403(10)	

[a]The calculated ADE for MnB_6^- is 2.43 eV at the B3LYP/6-311+G* level of theory.

bands or metastable electronic excited states of the anion (*vide infra*). The apparent enhancement of these weak signals in Figure 1a was due to the fact that the detachment cross section for peak X was reduced at the lower photon energy.

Computational Results. The lowest energy structure of MnB_6^- was found to be perfectly planar with C_{2v} symmetry (Figure 2). The structures and relative energies of other low-lying isomers within 1 eV of the global minimum are given in Figure S1. The ground state of MnB_6^- consists of a B-centered six-membered ring with Mn being on the periphery, similar to
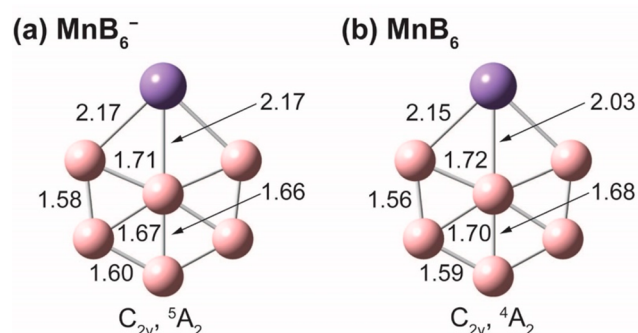
Figure 2. Optimized structures of (a) MnB_6^- and (b) MnB_6. The point group symmetries and electronic states are also given. The bond lengths are in Å.

the structure of ReB_6^-.[37] While ReB_6^- is closed shell, MnB_6^- is found to have a high spin state ($^5A_2$) with an electron configuration of $1a_1^2 1b_2^2 2a_1^2 2b_2^2 1b_1^2 3a_1^2 1a_2^2 3b_2^2 4a_1^2 4b_2^2$-$5a_1^2 6a_1^1 7a_1^1 2b_1^1 5b_2^1$. The occupied valence molecular orbitals (MO) are shown in Figure 3, where the β orbitals are also displayed for the doubly occupied π MOs since they show some differences from the corresponding α orbitals. The neutral ground state $^4A_2$ is obtained by detaching an α electron from the highest occupied MO (HOMO). As shown in Figure 2, there is a geometry change between the anion and the neutral ground state: the distance between the Mn atom and the central B atom is significantly shorter in the neutral. This is consistent with the removal of an electron from the HOMO, which exhibits an antibonding interaction between Mn and the central B atom.

■ DISCUSSION

Comparison of the Photoelectron Spectra of MnB_6^- with the Theoretical Results. The ADE of MnB_6^- is

calculated to be 2.43 eV at the B3LYP/6-311+G* level of theory, which agrees well with the experimental value of 2.4591 eV. The computed vibrational frequencies also show excellent agreement with the experimental measurements (Table 1). Five totally symmetric vibrational modes, v_6, v_5, v_4, v_3, and v_1, were observed and assigned to peaks a, b, d, e, and h, respectively. Their displacement vectors are given in Figure S2. As shown in the experimental spectra, the most Franck–Condon active mode is v_6, which corresponds to the stretching motion of the Mn atom. This observation is consistent with the fact that electron detached is from the HOMO of MnB_6^- (Figure 3). A Franck–Condon simulation was done,[59] as compared with the 2.6415 eV spectrum in Figure 4, which reproduced all the major vibrational features of the experimental spectra. The overall excellent agreement between the experimental and theoretical results confirms unequivocally the geometric and electronic structure of MnB_6^-.

The Franck–Condon simulation suggested that there were negligible vibrational hot band contributions to the weak signals below the 0–0 transition. These weak signals seemed to span a wide energy range down to ~2.2 eV. A very likely source of these weak signals was due to the population of low-lying electronic excited states of the anion. As shown in Figure S1, the $^7A_2$ excited state was computed to be ~0.22 eV above the $^5A_2$ ground state. Despite the fact that MnB_6^- was relatively cold vibrationally, the high-spin $^7A_2$ state, which was expected to be metastable, might not be in equilibrium with the vibrational temperature and could be populated in small quantity in the cluster beam.

Chemical Bonding and Aromaticity in MnB_6^-. Although MnB_6^- has a similar geometric structure as the recently reported ReB_6^-, their electronic structures are different. In MnB_6^-, due to its large spin multiplicity, the shapes of the α and β orbitals are not necessarily the same. Figure 5 displays the occupied π-MOs of MnB_6^-. The β orbitals are found to be more diffuse relative to their α
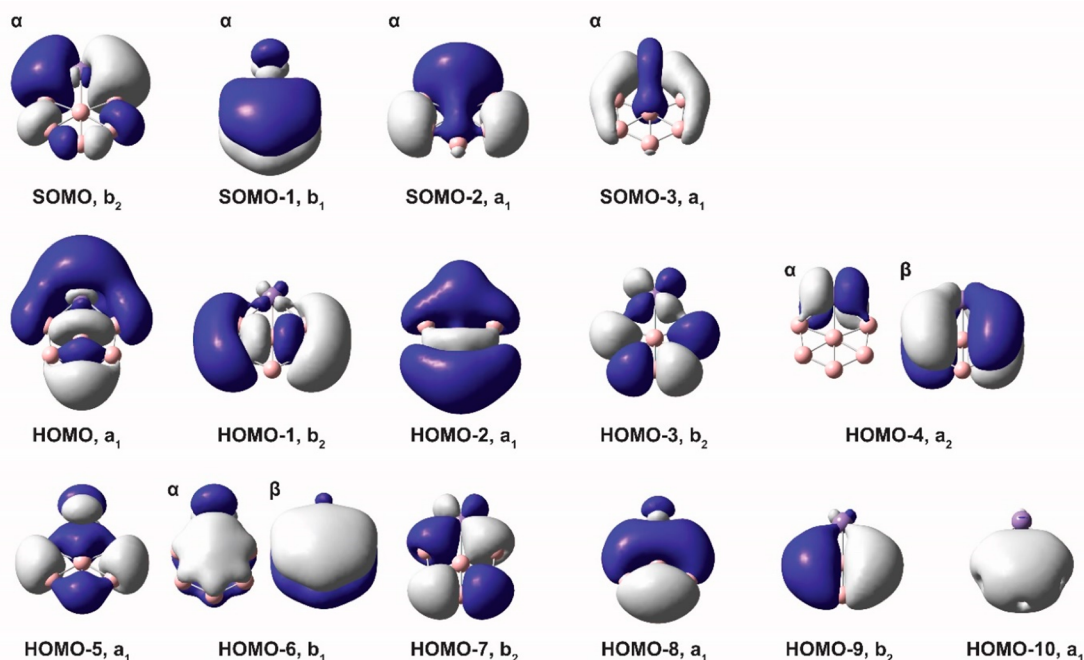

Figure 3. Occupied valence molecular orbitals of MnB_6^-. The α orbitals are displayed. The β orbitals for the doubly occupied π MOs are also shown.
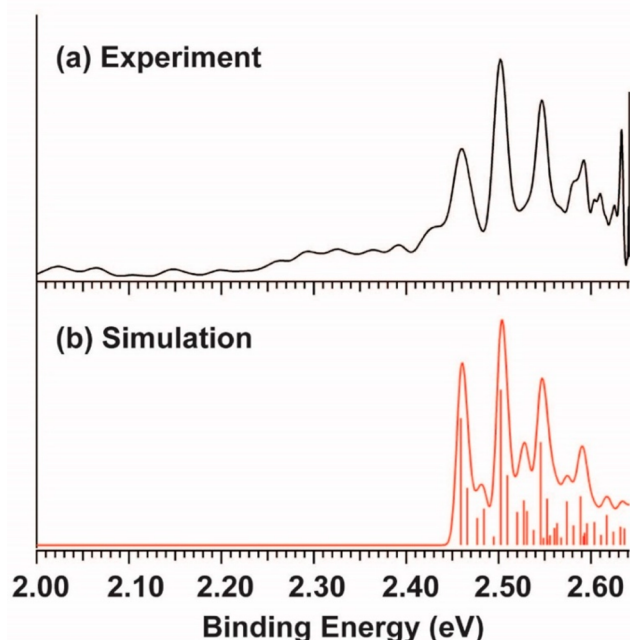
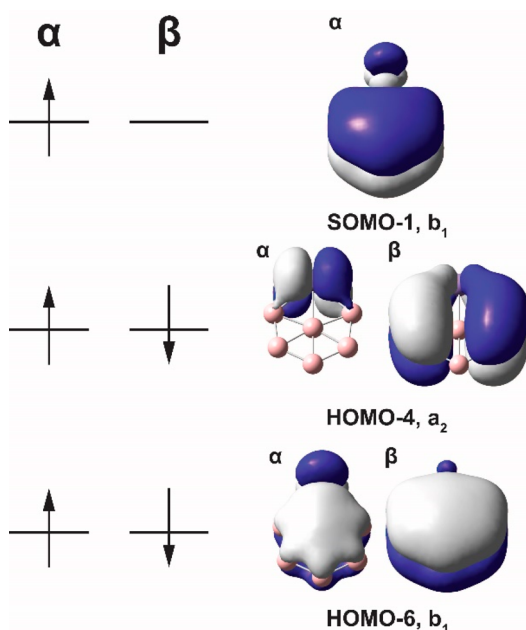**Figure 4.** Franck–Condon simulation of MnB_6^- at 100 K.

Figure 5. Occupied π-MOs of MnB_6^- at isovalue = 0.02 e/bohr.[3]

counterparts. In particular, the α electron in HOMO−4 is essentially localized in the $3d_{xz}$ orbital. On the other hand, the β orbital of HOMO−4 is mainly delocalized on the B atoms with a small contribution from the $3d_{xz}$ orbital. The π MOs of SOMO-1 and HOMO−6 are also mainly delocalized on the B_6 motif with relatively small contributions from the Mn 3d orbitals. In comparison to the 5d element Re, the 3d orbitals in Mn are spatially more contracted and are expected to have smaller overlap with the 2p orbitals of boron. The weaker bonding capacity of Mn with B can be gleaned from the significantly larger Mn−B bond distances (2.17 Å) in MnB_6^- (Figure 2a), compared with the Re−B bond distances (1.98− 2.05 Å) in ReB_6^-.[37] There have been two previous studies on

lanthanide hexaboride clusters (SmB_6^- and CeB_6^-),[62,63] which have similar planar structures as MnB_6^-. The Ln−B bond lengths are even longer, indicating even weaker interactions between the Ln atoms and boron in these clusters. In fact, the SmB_6^- cluster was characterized to consist of a B_6^{2-} unit with double antiaromaticity.[62]

Despite the fact that MnB_6^- possesses only five π electrons with one of the π MOs singly occupied, its structural similarity with ReB_6^- suggested that it might be aromatic, which was evaluated using the NICS index.[60,64] It should be noted that the open-shell nature of MnB_6^- makes it difficult to apply the Hückel rule. The $NICS(0)_{zz}$ and $NICS(1)_{zz}$ values of MnB_6^- were calculated at different sites (Figure S3) and are compared with those of benzene in Table 2. All of the the $NICS(0)_{zz}$ and

Table 2. $NICS(0)_{zz}$ and $NICS(1)_{zz}$ Values (in ppm) of Benzene and MnB_6^- at the B3LYP/6-311+G* Level of Theory[a]

$NICS(0)_{zz}$	site X	site A	site B	site C
C_6H_6	−14.07	−	−	−
MnB_6^-	−140.79	−31.40	−35.07	−32.34
$NICS(1)_{zz}$	site X	site A	site B	site C
C_6H_6	−29.06	−	−	−
MnB_6^-	−8.87	−4.24	−2.72	−5.40

[a]The site positions are shown in Figure S3.

$NICS(1)_{zz}$ values are negative, indicating that MnB_6^- indeed has aromatic characters. Because the three π MOs are not completely filled, MnB_6^- can be considered as an open-shell weak aromatic system or a 3d metallaboron analog of metallabenzenes. The weak bonding between Mn and the B_6 motif in MnB_6^- suggests that the 3d transition metals should also have weaker interactions with carbon in metallabenzenes, consistent with the challenges to synthesize such compounds.

■ CONCLUSIONS

In conclusion, we have produced and studied a 3d metallaboron cluster (MnB_6^-) using high-resolution photoelectron imaging and quantum chemical calculations. Vibrationally resolved photoelectron spectra were obtained and used to determine the structure of MnB_6^- by comparing them with the theoretical results. MnB_6^- was found to have a planar B-centered hexagonal structure with the Mn atom on the periphery and a high-spin ground state. Molecular orbital analyses and NCIS calculations suggest that MnB_6^- is aromatic and can be viewed as an open-shell metallaboron analog of 3d metallabenzenes.

■ ASSOCIATED CONTENT

ⓈⒾ Supporting Information

The Supporting Information is available free of charge at https://pubs.acs.org/doi/10.1021/acs.jpca.0c00949.

> The relative energies of low-lying isomers, the computed vibrational frequencies, and the site positions for the NICS calculations of MnB_6^- (PDF)

■ AUTHOR INFORMATION

Corresponding Author

Lai-Sheng Wang − *Department of Chemistry, Brown University, Providence, Rhode Island 02912, United States;* ⓞ orcid.org/ 0000-0003-1816-5738; Email: lai-sheng_wang@brown.edu

Authors

Ling Fung Cheung − *Department of Chemistry, Brown University, Providence, Rhode Island 02912, United States;* orcid.org/0000-0002-2308-8135

G. Stephen Kocheril − *Department of Chemistry, Brown University, Providence, Rhode Island 02912, United States;* orcid.org/0000-0003-1388-6472

Joseph Czekner − *Department of Chemistry, Brown University, Providence, Rhode Island 02912, United States*

Complete contact information is available at:
https://pubs.acs.org/10.1021/acs.jpca.0c00949

Notes

The authors declare no competing financial interest.

■ REFERENCES

(1) Lipscomb, W. N. The Boranes and Their Relatives. *Science* **1977**, *196*, 1047−1055.

(2) Zhai, H. J.; Wang, L. S.; Alexandrova, A. N.; Boldyrev, A. I. On the Electronic Structure and Chemical Bonding of B_5^- and B_5 by Photoelectron Spectroscopy and *Ab Initio* Calculations. *J. Chem. Phys.* **2002**, *117*, 7917−7924.

(3) Zhai, H. J.; Alexandrova, A. N.; Birch, K. A.; Boldyrev, A. I.; Wang, L. S. Hepta- and Octa-Coordinated Boron in Molecular Wheels of 8- and 9-Atom Boron Clusters: Observation and Confirmation. *Angew. Chem., Int. Ed.* **2003**, *42*, 6004−6008.

(4) Alexandrova, A. N.; Boldyrev, A. I.; Zhai, H. J.; Wang, L. S. All-Boron Aromatic Clusters as Potential New Inorganic Ligands and Building Blocks in Chemistry. *Coord. Chem. Rev.* **2006**, *250*, 2811−2866.

(5) Oger, E.; Crawford, N. R.; Kelting, R.; Weis, P.; Kappes, M. M.; Ahlrichs, R. Boron Cluster Cations: Transition from Planar to Cylindrical Structures. *Angew. Chem., Int. Ed.* **2007**, *46*, 8503−8506.

(6) Sergeeva, A. P.; Popov, I. A.; Piazza, Z. A.; Li, W. L.; Romanescu, C.; Wang, L. S.; Boldyrev, A. I. Understanding Boron through Size-Selected Clusters: Structure, Chemical Bonding, and Fluxionality. *Acc. Chem. Res.* **2014**, *47*, 1349−1358.

(7) Wang, L. S. Photoelectron Spectroscopy of Size-Selected Boron Clusters: From Planar Structures to Borophenes and Borospherenes. *Int. Rev. Phys. Chem.* **2016**, *35*, 69−142.

(8) Pan, S.; Barroso, J.; Jalife, S.; Heine, T.; Asmis, K. R.; Merino, G. Fluxional Boron Clusters: From Theory to Reality. *Acc. Chem. Res.* **2019**, *52*, 2732−2744.

(9) Zhai, H. J.; Kiran, B.; Li, J.; Wang, L. S. Hydrocarbon Analogues of Boron Clusters — Planarity, Aromaticity and Antiaromaticity. *Nat. Mater.* **2003**, *2*, 827−833.

(10) Zubarev, D. Y.; Boldyrev, A. I. Comprehensive Analysis of Chemical Bonding in Boron Clusters. *J. Comput. Chem.* **2007**, *28*, 251−268.

(11) Sergeeva, A. P.; Zubarev, D. Y.; Zhai, H. J.; Boldyrev, A. I.; Wang, L. S. A Photoelectron Spectroscopic and Theoretical Study of B_{16}^- and B_{16}^{2-}: An All-Boron Naphthalene. *J. Am. Chem. Soc.* **2008**, *130*, 7244−7246.

(12) Huang, W.; Sergeeva, A. P.; Zhai, H. J.; Averkiev, B. B.; Wang, L. S.; Boldyrev, A. I. A Concentric Planar Doubly π-Aromatic B_{19}^- Cluster. *Nat. Chem.* **2010**, *2*, 202−206.

(13) Sergeeva, A. P.; Piazza, Z. A.; Romanescu, C.; Li, W. L.; Boldyrev, A. I.; Wang, L. S. B_{22}^- and B_{23}^-: All-Boron Analogues of Anthracene and Phenanthrene. *J. Am. Chem. Soc.* **2012**, *134*, 18065−18073.

(14) Piazza, Z. A.; Hu, H. S.; Li, W. L.; Zhao, Y. F.; Li, J.; Wang, L. S. Planar Hexagonal B_{36} as a Potential Basis for Extended Single-Atom Layer Boron Sheets. *Nat. Commun.* **2014**, *5*, 3113.

(15) Boldyrev, A. I.; Wang, L. S. Beyond Organic Chemistry: Aromaticity in Atomic Clusters. *Phys. Chem. Chem. Phys.* **2016**, *18*, 11589−11605.

(16) Romanescu, C.; Galeev, T. R.; Li, W. L.; Boldyrev, A. I.; Wang, L. S. Aromatic Metal-Centered Monocyclic Boron Rings: Co©B_8^- and Ru©B_9^-. *Angew. Chem., Int. Ed.* **2011**, *50*, 9334−9337.

(17) Romanescu, C.; Galeev, T. R.; Li, W. L.; Boldyrev, A. I.; Wang, L. S. Transition-Metal-Centered Monocyclic Boron Wheel Clusters (M©B_n): A New Class of Aromatic Borometallic Compounds. *Acc. Chem. Res.* **2013**, *46*, 350−358.

(18) Li, W. L.; Xie, L.; Jian, T.; Romanescu, C.; Huang, X.; Wang, L. S. Hexagonal Bipyramidal $[Ta_2B_6]^{-/0}$ Clusters: B_6 Rings as Structural Motifs. *Angew. Chem., Int. Ed.* **2014**, *53*, 1288−1292.

(19) Popov, I. A.; Jian, T.; Lopez, G. V.; Boldyrev, A. I.; Wang, L. S. Cobalt-Centered Boron Molecular Drums with the Highest Coordination Number in the CoB_{16}^- Cluster. *Nat. Commun.* **2015**, *6*, 8654.

(20) Jian, T.; Li, W. L.; Popov, I. A.; Lopez, G. V.; Chen, X.; Boldyrev, A. I.; Li, J.; Wang, L. S. Manganese-Centered Tubular Boron Cluster − MnB_{16}^-: A New Class of Transition-Metal Molecules with High Coordination. *J. Chem. Phys.* **2016**, *144*, 154310.

(21) Li, W. L.; Jian, T.; Chen, X.; Chen, T. T.; Lopez, G. V.; Li, J.; Wang, L. S. The Planar CoB_{18}^- Cluster as a Motif for Metallo-Borophenes. *Angew. Chem., Int. Ed.* **2016**, *55*, 7358−7363.

(22) Jian, T.; Li, W. L.; Chen, X.; Chen, T. T.; Lopez, G. V.; Li, J.; Wang, L. S. Competition between Drum-like and Quasi-planar Structures in RhB_{18}^-: Motifs for Metallo-Boronanotubes or Metallo-Borophenes. *Chem. Sci.* **2016**, *7*, 7020−7027.

(23) Robinson, P. J.; Liu, G.; Ciborowski, S.; Martinez-Martinez, C.; Chamorro, J. R.; Zhang, X.; McQueen, T. M.; Bowen, K. H.; Alexandrova, A. N. Mystery of Three Borides: Differential Metal−Boron Bonding Governing Superhard Structures. *Chem. Mater.* **2017**, *29*, 9892−9896.

(24) Li, W. L.; Chen, X.; Jian, T.; Chen, T. T.; Li, J.; Wang, L. S. From Planar Boron Clusters to Borophenes and Metalloborophenes. *Nat. Rev. Chem.* **2017**, *1*, 0071.

(25) Jian, T.; Chen, X. N.; Li, S. D.; Boldyrev, A. I.; Li, J.; Wang, L. S. Probing the Structures and Bonding of Size-Selected Boron and Doped-Boron Clusters. *Chem. Soc. Rev.* **2019**, *48*, 3550−3591.

(26) Czekner, J.; Cheung, L. F.; Kocheril, G. S.; Kulichenko, M.; Boldyrev, A. I.; Wang, L. S. High-Resolution Photoelectron Imaging of IrB_3^-: Observation of a π-Aromatic B_3^+ Ring Coordinated to a Transition Metal. *Angew. Chem., Int. Ed.* **2019**, *58*, 8877−8881.

(27) Ren, M.; Jin, S.; Wei, D.; Jin, Y.; Tian, Y.; Lu, C.; Gutsev, G. L. NbB_{12}^-: A New Member of Half-Sandwich Type Doped Boron Clusters with High Stability. *Phys. Chem. Chem. Phys.* **2019**, *21*, 21746−51752.

(28) Liu, X.; Zhao, G.; Guo, L.; Jing, Q.; Luo, Y. Structural, Electronic, and Magnetic Properties of MB_n (M = Cr, Mn, Fe, Co, Ni, n⩽7) Clusters. *Phys. Rev. A: At., Mol., Opt. Phys.* **2007**, *75*, 063201.

(29) Pu, Z.; Ito, K.; Schleyer, P. v. R.; Li, Q. S. Planar Hepta-, Octa-, Nona-, and Decacoordinate First Row d-Block Metals Enclosed by Boron Rings. *Inorg. Chem.* **2009**, *48*, 10679−10686.

(30) Yang, Z.; Xiong, S. J. Structures and Electronic Properties of Small FeB_n (n = 1−10) Clusters. *J. Chem. Phys.* **2008**, *128*, 184310.

(31) Ge, G.; Jing, Q.; Cao, H.; Yan, H. Structural, Electronic, and Magnetic Properties of MB_n (M = Y, Zr, Nb, Mo, Tc, Ru, n ⩽ 8) Clusters. *J. Cluster Sci.* **2012**, *23*, 189−202.

(32) Zhao, X. Y.; Luo, X. M.; Tian, X. X.; Lu, H. G.; Li, S. D. NiB_{10}, NiB_{11}^-, NiB_{12}, and NiB_{13}^+: Half-Sandwich Complexes with the Universal Coordination Bonding Pattern of σ Plus π Double Delocalization. *J. Cluster Sci.* **2019**, *30*, 115−121.

(33) Xu, C.; Cheng, L.; Yang, J. Double Aromaticity in Transition Metal Centered Double-Ring Boron Clusters M@B_{2n} (M = Ti, Cr, Fe, Ni, Zn; n = 6, 7, 8). *J. Chem. Phys.* **2014**, *141*, 124301.

(34) Pham, H. T.; Nguyen, M. T. Effects of Bimetallic Doping on Small Cyclic and Tubular Boron Clusters: B_7M_2 and $B_{14}M_2$ Structures with M = Fe, Co. *Phys. Chem. Chem. Phys.* **2015**, *17*, 17335−17345.

(35) Zhao, L.; Qu, X.; Wang, Y.; Lv, J.; Zhang, L.; Hu, Z.; Gu, G.; Ma, Y. Effects of Manganese Doping on the Structure Evolution of Small-Sized Boron Clusters. *J. Phys.: Condens. Matter* **2017**, *29*, 265401.

(36) Chen, T. T.; Li, W. L.; Bai, H.; Chen, W. J.; Dong, X. R.; Li, J.; Li; Wang, L. S. Re©B$_8^-$ and Re©B$_9^-$: New Members of the Transition-Metal-Centered Borometallic Molecular Wheel Family. *J. Phys. Chem. A* **2019**, *123*, 5317−5324.

(37) Cheung, L. F.; Czekner, J.; Kocheril, G. S.; Wang, L. S. ReB$_6^-$: A Metallaboron Analog of Metallabenzenes. *J. Am. Chem. Soc.* **2019**, *141*, 17854−17860.

(38) Thorn, D. L.; Hoffmann, R. Delocalization in Metallocycles. *Nouv. J. Chim.* **1979**, *3*, 39−45.

(39) Bleeke, J. R. Metallabenzenes. *Chem. Rev.* **2001**, *101*, 1205−1228.

(40) Frogley, B. J.; Wright, L. J. Recent Advances in Metallaaromatic Chemistry. *Chem. - Eur. J.* **2018**, *24*, 2025−2038.

(41) Fernández, I.; Frenking, G.; Merino, G. Aromaticity of Metallabenzenes and Related Compounds. *Chem. Soc. Rev.* **2015**, *44*, 6452−6463.

(42) Elliott, G. P.; Roper, W. R.; Waters, J. M. Metallacyclohexatrienes or 'Metallabenzenes.' Synthesis of Osmabenzene Derivatives and *X*-ray Crystal Structure of [Os(CSCHCHCHCH)(CO)(PPh$_3$)$_2$]. *J. Chem. Soc., Chem. Commun.* **1982**, 811−813.

(43) Bleeke, J. R.; Behm, R.; Xie, Y. F.; Chiang, M. Y.; Robinson, K. D.; Beatty, A. M. Synthesis, Structure, Spectroscopy, and Reactivity of a Metallabenzene. *Organometallics* **1997**, *16*, 606−623.

(44) Jacob, V.; Weakley, T. J. R.; Haley, M. M. Metallabenzenes and Valence Isomers. Synthesis and Characterization of a Platinabenzene. *Angew. Chem., Int. Ed.* **2002**, *41*, 3470−3473.

(45) Gilbertson, R. D.; Lau, T. L. S.; Lanza, S.; Wu, H. P.; Weakley, T. J. R.; Haley, M. M. Synthesis, Spectroscopy, and Structure of a Family of Iridabenzenes Generated by the Reaction of Vaska-Type Complexes with a Nucleophilic 3-Vinyl-1-cyclopropene. *Organometallics* **2003**, *22*, 3279−3289.

(46) Paneque, M.; Posadas, C. M.; Poveda, M. L.; Rendón, N.; Salazar, V.; Oñate, E.; Mereiter, K. Formation of Unusual Iridabenzene and Metallanaphthalene Containing Electron-Withdrawing Substituents. *J. Am. Chem. Soc.* **2003**, *125*, 9898−9899.

(47) Poon, K. C.; Liu, L.; Guo, T.; Li, J.; Sung, H. H. Y.; Williams, I. D.; Lin, Z.; Jia, G. Synthesis and Characterization of Rhenabenzenes. *Angew. Chem., Int. Ed.* **2010**, *49*, 2759−2762.

(48) Yang, J.; Jones, W. M.; Dixon, J. K.; Allison, N. T. Detection of a Ruthenabenzene, Ruthenaphenoxide, and Ruthenaphenanthrene Oxide: The First Metalla Aromatics of a Second-Row Transition Metal. *J. Am. Chem. Soc.* **1995**, *117*, 9776−9777.

(49) Zhang, H.; Xia, H.; He, G.; Wen, T. B.; Gong, L.; Jia, G. Synthesis and Characterization of Stable Ruthenabenzenes. *Angew. Chem., Int. Ed.* **2006**, *45*, 2920−2923.

(50) Lin, R.; Zhang, H.; Li, S.; Wang, J.; Xia, H. New Highly Stable Metallabenzenes via Nucleophilic Aromatic Substitution Reaction. *Chem. - Eur. J.* **2011**, *17*, 4223−4231.

(51) Zhang, Y.; Wei, J.; Zhu, M.; Chi, Y.; Zhang, W. X.; Ye, S.; Xi, Z. Tetralithio Metalla-Aromatics with Two Independent Perpendicular Dilithio Aromatic Rings Spiro-fused by One Manganese Atom. *Angew. Chem.* **2019**, *131*, 9727−9733.

(52) Lin, M.; Li, P.; Cao, Z. Effects of Structural Modification on the Ground State of Metallabenzenes: Singlet versus Triplet State. *J. Theor. Comput. Chem.* **2011**, *10*, 861−874.

(53) León, I.; Yang, Z.; Liu, H. T.; Wang, L. S. The Design and Construction of a High-Resolution Velocity-Map Imaging Apparatus for Photoelectron Spectroscopy Studies of Size-Selected Clusters. *Rev. Sci. Instrum.* **2014**, *85*, 083106.

(54) Dick, B. Inverting Ion Images without Abel Inversion: Maximum Entropy Reconstruction of Velocity Maps. *Phys. Chem. Chem. Phys.* **2014**, *16*, 570−580.

(55) Perdew, J. P.; Burke, K.; Ernzerhof, M. Generalized Gradient Approximation Made Simple. *Phys. Rev. Lett.* **1996**, *77*, 3865−3868.

(56) Dill, J. D.; Pople, J. A. Self-consistent molecular orbital methods. XV. Extended Gaussian-Type Basis Sets for Lithium, Beryllium, and Boron. *J. Chem. Phys.* **1975**, *62*, 2921−2923.

(57) Rassolov, V. A.; Pople, J. A.; Ratner, M. A.; Windus, T. L. M. 6-31G* Basis Set for Atoms K through Zn. *J. Chem. Phys.* **1998**, *109*, 1223−1229.

(58) Becke, A. D. Density-Functional Thermochemistry. III. The Role of Exact Exchange. *J. Chem. Phys.* **1993**, *98*, 5648−5652.

(59) Mozhayskiy, V. A.; Krylov, A. I. *ezSpectrum*. http://iopenshell. usc.edu/downloads (accessed March 21, 2019).

(60) Schleyer, P. v. R.; Maerker, C.; Dransfeld, A.; Jiao, H.; van Eikema Hommes, N. J. R. Nucleus-Independent Chemical Shifts: A Simple and Efficient Aromaticity Probe. *J. Am. Chem. Soc.* **1996**, *118*, 6317−6318.

(61) Frisch, M. J.; Trucks, G. W.; Schlegel, H. B.; Scuseria, G. E.; Robb, M. A.; Cheeseman, J. R.; Scalmani, G.; Barone, V.; Mennucci, B.; Petersson, G. A.; et al. *Gaussian 09*, Revision C.01; Gaussian, Inc.: Wallingford, CT, 2009.

(62) Robinson, P. J.; Zhang, X.; McQueen, T.; Bowen, K. H.; Alexandrova, A. N. SmB$_6^-$ Cluster Anion: Covalency Involving f Orbitals. *J. Phys. Chem. A* **2017**, *121*, 1849−1854.

(63) Mason, J. L.; Harb, H.; Huizenga, C. D.; Ewigleben, J. C.; Topolski, J. E.; Hratchian, H. P.; Jarrold, C. C. Electronic and Molecular Structures of the CeB$_6$ Monomer. *J. Phys. Chem. A* **2019**, *123*, 2040−2048.

(64) Fallah-Bagher-Shaidaei, H.; Wannere, C. S.; Corminboeuf, C.; Puchta, R.; Schleyer, P. v. R. Which NICS Aromaticity Index for Planar π Rings Is Best? *Org. Lett.* **2006**, *8*, 863−866.